

# Sensitivity of Hongmeng 21cm experiment on scattering dark matter

Junsong Cang<sup>1,2</sup> , Yu Gao<sup>3</sup> , and Yin-Zhe Ma<sup>4,5</sup> 

<sup>1</sup> Theoretical and Scientific Data Science, Scuola Internazionale Superiore di Studi Avanzati (SISSA), Via Bonomea 265, 34136 Trieste, Italy

<sup>2</sup> Scuola Normale Superiore, Piazza dei Cavalieri 7, 56126 Pisa, Italy

<sup>3</sup> State Key Laboratory of Particle Astrophysics, Institute of High Energy Physics, Chinese Academy of Sciences, Beijing, 100049, China

<sup>4</sup> Department of Physics, Stellenbosch University, Matieland 7602, South Africa

<sup>5</sup> National Institute for Theoretical and Computational Sciences (NITheCS), Stellenbosch University, Matieland 7602, South Africa

Received XXXX; accepted XXXX

## ABSTRACT

Scattering between dark matter and baryon can cool intergalactic medium temperature and deepen the 21cm signal. Such interactions have been proposed to explain the unusually deep 21cm absorption signal reported by EDGES in 2018. This paper explores the potential to detect dark matter - baryon scattering with the Hongmeng project, an upcoming lunar orbiting satellite experiment dedicated to measuring global 21cm signal between redshifts 11 – 46. We self-consistently forward-model the simulated sky temperature data, jointly varying both the astrophysical and foreground models. We show that even with a very conservative observational strategy in which the experiment only takes data when both the Earth and the Sun are shielded by the Moon, Hongmeng can tighten the current constraints on dark matter - baryon scattering cross-section  $\sigma_0$  by a factor of 21 after the full mission which lasts for five years. The prospective upper limit on  $\sigma_0$  can reach  $4 \times 10^{-43} \text{ cm}^2$  for dark matter masses between 0.1 MeV and 0.4 GeV. Even after only one month of observation, a factor of 3 improvement relative to current  $\sigma_0$  limits can be expected.

**Key words.** Cosmology: theory, early Universe, dark ages, reionization, first stars, dark matter

## 1. Introduction

Redshifted 21cm signals hold the potential to revolutionize cosmology with the promises of mapping out the first half of our observable Universe. The first claim of 21cm signal detection was reported by the EDGES experiment in 2018 (Bowman et al. 2018), featuring a global (i.e., spatially averaged) absorption signal centered at redshift 17 with a depth of  $\sim 500$  mK, approximately twice as deep as the most optimistic astrophysical prediction in which the cosmic microwave background (CMB) dominates the radio background and the intergalactic gas cools adiabatically. Such deep signal can be achieved by either a radio background in excess of CMB (Feng & Holder 2018; Ewall-Wice et al. 2018; Fialkov & Barkana 2019; Mirocha & Furlanetto 2019; Ewall-Wice et al. 2020; Reis et al. 2020; Cang et al. 2025), or excess gas cooling via scattering between dark matter (DM) and baryon (Muñoz & Loeb 2018; Barkana 2018). Early dark energy can also achieve additional cooling needed to reproduce the EDGES depth, however such models are strongly ruled out by other cosmological observations (Hill & Baxter 2018), e.g., CMB anisotropy spectrum (Karwal & Kamionkowski 2016), measurements of Hubble constant (Riess et al. 2018).

Dark matter decouples much earlier than baryon owing to its extremely weak, or even entirely absent, interactions with Standard Model particles, and its temperature therefore remains much lower than that of baryons throughout cosmic history. In a scattering dark matter (SDM) framework, DM may interact with baryons through elastic scattering and this allows some heat

transfer from baryons to DM, leading to excess cooling of the gas and consequently a deepened 21cm absorption signal that can potentially reproduce the depth reported by EDGES, provided that a strong Lyman-alpha background was present to couple the gas spin temperature to its kinetic temperature (Muñoz & Loeb 2018; Barkana 2018). In addition to deepening the global signal, cooling from SDM can also enhance 21cm fluctuation (Muñoz et al. 2018), offering promising prospects for experiments dedicated to measure 21cm power spectrum (Rahimieh et al. 2025), e.g., Square Kilometre Array (SKA; e.g., Mellema et al. 2013), Hydrogen Epoch of Reionization Array (HERA; Abdurashidova et al. 2022), Low Frequency Array (LOFAR; van Haarlem et al. 2013). Models to achieve such interactions generally fall into two categories (Flitter & Kovetz 2024): (i) millicharged models (McDermott et al. 2011; Muñoz & Loeb 2018; Kovetz et al. 2018; Berlin et al. 2018; Barkana et al. 2018; Slatyer & Wu 2018; Liu & Slatyer 2018; Falkowski & Petraki 2018; Muñoz et al. 2018; Driskell et al. 2022), which require SDM to carry fractional electrical charge and interact only with charged particles, i.e., free electrons and protons; (ii) baryophilic models (Dvorkin et al. 2014; Muñoz et al. 2015; Boddy et al. 2018; Fialkov et al. 2018; Xu et al. 2018; Short et al. 2022; He et al. 2023), in which case SDM interact with all standard model particles.

However, despite the excitement surrounding possible discovery, there are concerns about the modeling of EDGES data. Hills et al. (2018) pointed out that the parameters of foreground model that EDGES used to model their data have unphysical values. The phenomenological Flat-Gaussian 21cm model applied in the original analysis was highly unlikely for any realistic

\* cangjunsong@outlook.com

astrophysical models without resorting to extreme fine-tuning (Gessey-Jones et al. 2023; Nelander et al. 2025). Sims & Pober (2020) and Cang et al. (2025) suggested that there could be calibration residuals in EDGES sky temperature data and that after consistently forward modeling the data with physically motivated models for cosmic 21cm signal, foreground and calibration, the inferred 21cm signal was in fact entirely consistent with that expected from standard model. Furthermore, subsequent measurement made by the SARAS3 experiment (Singh et al. 2022; Bevins et al. 2022) pointed to a non-detection of a cosmic 21cm signal.

A robust detection of the 21 cm signal remains extremely challenging due to the complex interplay of astrophysical and terrestrial foregrounds, which are typically orders of magnitude brighter than the cosmological signal itself (Pritchard & Loeb 2012; Hibbard et al. 2023). Reliable measurements therefore require a careful joint characterization of the cosmic signal, foregrounds, and instrumental effects, along with validations from independent observations. Ground based global spectrum experiments such as EDGES (Bowman et al. 2018), SARAS (Singh et al. 2022; Bevins et al. 2022) and LEDA (Large Aperture Experiment to Detect the Dark Ages, Greenhill & Bernardi 2012) are susceptible to various terrestrial contaminations (Shi et al. 2022), e.g., attenuation, refraction and attenuation of the radio wave by Earth ionosphere (Vedantham et al. 2014; Shen et al. 2021; Chen et al. 2023), antenna interactions with the nearby environment (Shi et al. 2022), and radio frequency interference (RFI) (Tauscher et al. 2020), all of which makes precise measurement of 21cm signal even more difficult. Several space borne missions have been proposed to circumvent these issues, e.g., Dark Ages Polarimetry Pathfinder (DAPPER; Tauscher et al. 2018) Dark Ages Radio Explorer (DARE, Burns et al. 2017), Farside Array for Radio Science Investigations of the Dark ages and Exoplanets (FARSIDE, Burns et al. 2021; Burns et al. 2021) and Hongmeng (also known as Discovering the Sky at the Longest wavelength or DSL) (Chen et al. 2019, 2020; Shi et al. 2022; Chen et al. 2023).

Designed to operate on a lunar orbit, the Hongmeng mission (Chen et al. 2019, 2020; Shi et al. 2022; Chen et al. 2023) is naturally free from ionosphere contamination, and most importantly the Moon can serve as a natural shield against RFI contamination from the Earth, which remains a major challenge even for Earth orbiting satellites. Hongmeng is designed to measure 21cm signal in a broad redshift window of  $11 \lesssim z \lesssim 46$  (Chen et al. 2020), reaching deep into the cosmic dark ages while encompassing the onset of reionization. New physics processes such as DM–baryon scattering may operate during the dark ages, well before the onset of astrophysical heating. The ability to explore this pristine epoch places Hongmeng in a particularly advantageous position to provide a clean probe of new physics, free from astrophysical uncertainties, and it has been shown in Zhao et al. (2025) that, with a modest observing time, Hongmeng could potentially constrain DM annihilation and decay, as well as Hawking radiation from primordial black holes, with a precision exceeding current leading limits by orders of magnitude.

This work investigates the potential of Hongmeng in probing DM-baryon scattering. We will consistently forward model both the cosmic signal and foreground. The rest of this paper is organised as follows: we briefly review 21cm signal and impact of SDM in Sect. 2, our forecast pipeline is detailed in Sect. 3, we show our results in Sect. 4 and finally we conclude in Sect. 5. We use standard  $\Lambda$ CDM cosmology throughout with the relevant cosmological parameters set by Planck 2018 results (Aghanim et al. 2020):  $h = 0.6766$ ,  $\Omega_b h^2 = 0.02242$ ,  $\Omega_c h^2 = 0.11933$ ,  $\ln(10^{10} A_s) = 3.047$ ,  $n_s = 0.9665$ .

## 2. 21cm signal with Scattering Dark Matter

In cosmological context, the strength of 21cm signal is measured by its differential brightness temperature  $T_{21}$  (referred to as 21cm temperature hereafter for simplicity). Ignoring the spatial fluctuations, global  $T_{21}$  can be approximated as (Furlanetto & Briggs 2004; Mesinger et al. 2011; Pritchard & Loeb 2012; Sitwell et al. 2014),

$$T_{21} \approx 27x_H \left(1 - \frac{T_R}{T_s}\right) \left(\frac{1+z}{10}\right)^{1/2} \left(\frac{0.15}{\Omega_m h^2}\right) \left(\frac{\Omega_b h^2}{0.023}\right) \text{mK}, \quad (1)$$

here  $x_H$  is hydrogen neutral fraction,  $T_R$  is the radio background temperature and is assumed to be dominated by CMB in this work such that  $T_R = T_{\text{CMB}}$  and  $T_{\text{CMB}} = 2.728(1+z)$  K is the CMB temperature.  $\Omega_m$  and  $\Omega_b$  are fractional energy density in matter and baryon respectively,  $h$  is the Hubble constant in unit of  $100 \text{km s}^{-1} \text{Mpc}^{-1}$ , finally the spin temperature  $T_s$  is coupled to baryonic intergalactic medium (IGM) kinetic temperature  $T_k$  and radio background temperature  $T_R$  by (Pritchard & Loeb 2012; Sitwell et al. 2014),

$$T_s^{-1} = \frac{T_R^{-1} + x_\alpha T_\alpha^{-1} + x_c T_k^{-1}}{1 + x_\alpha + x_c}, \quad (2)$$

where  $T_\alpha \approx T_k$  is the color temperature (Hirata 2006), and  $x_c$  and  $x_\alpha$  are the collisional and Wouthuysen-Field coupling coefficients respectively (see Pritchard & Loeb 2012).

We use the publicly available 21cmFirstCLASS code (Flitter & Kovetz 2024) to compute 21cm signal. 21cmFirstCLASS uses a modified version of CLASS (Blas et al. 2011; Gluscevic & Boddy 2018; Boddy & Gluscevic 2018; Nguyen et al. 2021; Boddy et al. 2022) code to compute the initial conditions in the presence of SDM. These are then passed to a modified version of 21cmFAST (Mesinger et al. 2011; Park et al. 2019; Murray et al. 2020), highly customized to incorporate SDM cooling while maintaining the original astrophysical framework, which solves for various components required to calculate  $T_{21}$ . Below we give a minimalist review of essential ingredients related to SDM cooling in 21cmFirstCLASS and astrophysical background in 21cmFAST, and we refer interested readers to Flitter & Kovetz (2024) and Mesinger et al. (2011); Murray et al. (2020); Qin et al. (2020); Muñoz et al. (2022) for full details.

### 2.1. Scattering dark matter

We consider a Coulomb-like interaction (Boddy & Gluscevic 2018; Slatyer & Wu 2018; Lin & Gao 2026) that is enhanced at low red-shift. In this case, DM-baryon scattering cross-section  $\sigma$  takes the form,

$$\sigma = \sigma_0 \left(\frac{v}{c}\right)^{-4}, \quad (3)$$

here  $c$  is the speed of light,  $v$  is the relative velocity between SDM and baryon,  $\sigma_0$  normalizes the cross-section and is treated as a free parameter. SDM impacts 21cm signal primarily by changing IGM temperature  $T_k$  in Eq. (2). In presence of SDM, the evolution equation of IGM temperature can be schematically written as (Flitter & Kovetz 2024),

$$\frac{dT_k}{dt} = \left.\frac{dT_k}{dt}\right|_{\text{cosmo}} + \left.\frac{dT_k}{dt}\right|_{\text{astro}} + \left.\frac{dT_k}{dt}\right|_{\text{SDM}}, \quad (4)$$

where  $dT_k/dz|_{\text{cosmo}}$  contains the cosmological contributions from Compton heating, and adiabatically cooling due to cosmic

expansion,  $dT_k/dz|_{\text{astro}}$  describes the X-ray heating from astrophysical sources in 21cmFAST (Mesinger et al. 2011; Park et al. 2019; Murray et al. 2020), and  $dT_k/dz|_{\text{SDM}}$  is the evolution rate from SDM (Flitter & Kovetz 2024),

$$\left. \frac{dT_k}{dt} \right|_{\text{SDM}} = \Gamma_\chi (T_\chi - T_k) + \frac{2}{3k_B} \frac{\rho_\chi v}{\rho_b + \rho_\chi} \sum_t \frac{m_\chi m_b}{m_\chi + m_t} D_t(v), \quad (5)$$

here the subscript  $\chi$  represents SDM particle,  $m_\chi$  and  $T_\chi$  are mass and temperature of SDM,  $\rho_b$  and  $\rho_\chi$  are energy densities in baryon and SDM respectively. For simplicity we assume that all DM consists of SDM, thus  $\rho_\chi = \Omega_c \rho_{\text{cr}} (1+z)^3$ , where  $\Omega_c$  is the fractional DM density,  $\rho_{\text{cr}}$  is the critical density today.  $k_B$  is Boltzmann's constant,  $m_b = m_H / [x_H (1 - (1 - m_H/m_{\text{He}})Y_{\text{He}})]$  is the mean baryon mass, where  $m_H$  and  $m_{\text{He}}$  are the masses of hydrogen and helium atoms respectively,  $Y_{\text{He}} \approx 0.245$  is the helium mass fraction. The subscript  $t$  indicates target particle that SDM interacts with. We assume baryophilic scenario (Dvorkin et al. 2014; Muñoz et al. 2015; Boddy et al. 2018; Fialkov et al. 2018; Xu et al. 2018; Short et al. 2022; He et al. 2023) in which SDM interacts with all standard model particles.

Finally in Eq. (5)  $\Gamma_\chi$  and  $D_t$  represent the energy transfer rate and the mutual drag force acting on SDM-baryon fluids, respectively (Flitter & Kovetz 2024),

$$\Gamma_\chi = \sqrt{\frac{2}{\pi}} \frac{2\sigma_0 c^4 \rho_\chi}{3n_b} \sum_t \frac{\rho_t \exp(-r_t^2/2)}{(m_t + m_\chi)^2} u_{\chi t}^3, \quad (6)$$

$$D_t = \frac{(\rho_b + \rho_\chi) \sigma_0 c^4}{\rho_b u_{\chi t}^2} \frac{\rho_t F(r_t)}{m_t + m_\chi} \quad (7)$$

here  $n_b = \rho_b/m_b$  is the baryon number density,  $r_t = v/u_{\chi t}$  where  $u_{\chi t}$  is the thermal velocity,  $F(r_t) = r_t^{-2} \left[ \text{erf}\left(\frac{r_t}{\sqrt{2}}\right) - \sqrt{\frac{2}{\pi}} r_t e^{-r_t^2/2} \right]$ .

Equation (5) shows that SDM can either cool or heat the IGM. When the SDM temperature is much lower than that of the baryons, the energy transfer between them acts as a coolant, lowering the IGM temperature. However, if there exists a non-negligible relative velocity between SDM and baryons, the frictional dissipation between the two fluids can heat both components, therefore in some cases SDM may actually heat the baryons if the frictional heating is strong enough (Muñoz et al. 2015). We discuss this further in Sect. 4.

## 2.2. Astrophysical background

We assume that stars form in both population II (Pop II) and population III (Pop III) galaxies. In 21cmFAST, these galaxies are classified depending on their gas accretion mechanisms (Qin et al. 2020; Muñoz et al. 2022). The metal poor Pop III galaxies accrete gas mainly by rotational-vibrational transitions of hydrogen molecules, whereas Pop II galaxies are typically made from metallic remnants of Pop III galaxies and they obtain gas primarily through line transitions of hydrogen atoms.

Astrophysical sources affect the 21cm signal mainly through three radiative processes: (i) IGM heating by X-ray; (ii) ionization by UV photons; and (iii) Lyman-alpha radiation, which couples  $T_s$  to  $T_k$  via Wouthuysen-Field (WF) effects. All these radiation fields trace star formation history (Fragos et al. 2013b; Park et al. 2019). To account for these uncertainties, we adopt the astrophysical framework detailed in Muñoz et al. (2022) and vary

the following 21cmFAST astrophysical parameters (in addition to the SDM parameters  $m_\chi$  and  $\sigma_0$ ):

$$\{f_{\star,10}, \alpha_{\star,\text{II}}, f_{\star,7}, \alpha_{\star,\text{III}}, \mathcal{L}_{\text{X,II}}, \mathcal{L}_{\text{X,III}}, f_{\text{esc},10}, f_{\text{esc},7}\} \quad (8)$$

Together these parameters describe the star formation, X-ray and UV radiations of Pop II and Pop III galaxies. We briefly review these parameters below and we refer interested readers to Qin et al. (2020); Muñoz et al. (2022) for extensive discussions.

### 2.2.1. Star formation

In 21cmFAST, the stellar fraction  $f_\star$ , which describes the fraction of halo baryonic mass converted into stars, is modelled in Pop II and Pop III galaxies as,

$$f_{\star,\text{II}} = \min \left[ f_{\star,10} \left( \frac{M_h}{10^{10} M_\odot} \right)^{\alpha_{\star,\text{II}}}, 1 \right], \quad (9)$$

$$f_{\star,\text{III}} = \min \left[ f_{\star,7} \left( \frac{M_h}{10^7 M_\odot} \right)^{\alpha_{\star,\text{III}}}, 1 \right], \quad (10)$$

where  $M_h$  is DM halo mass, the subscripts II and III denote Pop II and Pop III galaxies respectively.  $f_{\star,10}$ ,  $f_{\star,7}$ ,  $\alpha_{\star,\text{II}}$  and  $\alpha_{\star,\text{III}}$  are free parameters describing the normalization and power index of stellar fraction. Because X-ray, Lyman- $\alpha$ , and UV radiation fields are all sourced by star formation, a higher star formation rate (SFR) accelerates the WF coupling, X-ray heating, and reionization. As a result, when increasing SFR the 21-cm signal becomes deeper prior to the X-ray heating era (due to stronger WF coupling that ties  $T_s$  to the cold IGM), but becomes shallower afterwards due to enhanced X-ray heating and UV ionization.

### 2.2.2. X-ray radiation

X-rays from galaxies are mainly emitted by high mass X-ray binaries (HMXBs) (Fragos et al. 2013b). Because these systems have relatively short lifetimes, their comoving X-ray emissivity  $\epsilon_X$  traces star formation rate density (SFRD) (Cang et al. 2025),

$$\epsilon_X = L_X / \text{SFR} \times \text{SFRD}, \quad (11)$$

here  $L_X / \text{SFR}$  denotes the monochromatic X-ray luminosity per SFR and is assumed to follow a power-law energy spectrum. Normalizations of  $L_X / \text{SFR}$  below 2 keV is treated as a free parameter  $\mathcal{L}_X$  in 21cmFAST,

$$\mathcal{L}_{\text{X,II}} \equiv \int_{E_0}^{2\text{keV}} dE L_{\text{X,II}} / \text{SFR}, \quad (12)$$

$$\mathcal{L}_{\text{X,III}} \equiv \int_{E_0}^{2\text{keV}} dE L_{\text{X,III}} / \text{SFR}, \quad (13)$$

where  $E_0 = 0.5$  keV is the threshold energy below which photons are absorbed within the host galaxy (Das et al. 2017). Following Park et al. (2019), we adopt fiducial values of  $\mathcal{L}_{\text{X,II}} = \mathcal{L}_{\text{X,III}} = 10^{40.5} \text{ergs}^{-1} M_\odot^{-1} \text{yr}$ , which is consistent with HMXBs simulations in metal-poor environments (Fragos et al. 2013a).

X-rays affect the 21cm signal primarily through heating, and increasing  $\mathcal{L}_{\text{X,II}}$  and  $\mathcal{L}_{\text{X,III}}$  raises both the kinetic and spin temperatures ( $T_k$  and  $T_s$ ), shifting the 21 cm signal from absorption to emission and moving the absorption trough to higher redshifts while enhancing the emission amplitude. A fraction of the X-ray energy not deposited as heat can contribute to ionization and to the Lyman-alpha background (Qin et al. 2020), thereby accelerating both reionization and WF coupling.



**Table 1.** Parameters varied in our forecast and their fiducial values.

Parameters	Eq.	Units	Flat prior	Fiducial
$\sigma_0$	3	$\text{cm}^2$	linear	0
$m_\chi$	5	GeV	-	-
$f_{\star,10}$	9	-	$\log_{10}$	0.05
$f_{\text{esc},10}$	14	-	$\log_{10}$	0.1
$\mathcal{L}_{\text{X,II}}$	12	$\text{erg s}^{-1} \text{M}_\odot^{-1} \text{yr}$	$\log_{10}$	$10^{40.5}$
$\alpha_{\star,\text{II}}$	9	-	linear	0.5
$f_{\star,7}$	10	-	$\log_{10}$	0.05
$f_{\text{esc},7}$	15	-	$\log_{10}$	0.1
$\mathcal{L}_{\text{X,III}}$	13	$\text{erg s}^{-1} \text{M}_\odot^{-1} \text{yr}$	$\log_{10}$	$10^{40.5}$
$\alpha_{\star,\text{III}}$	10	-	linear	0.5
$p_0$	17	K	linear	1697.81
$p_{1-4}$	17	K	linear	0

### 2.2.3. Ionizing UV background

The epoch of reionization is thought to be driven mainly by UV photons (Furlanetto et al. 2006). Similar to the stellar fraction in Eqs. (9) and (10), the escape fraction  $f_{\text{esc}}$ —the fraction of ionizing UV photons that escape their host galaxies and contribute to the reionization of IGM—is modeled in 21cmFAST as,

$$f_{\text{esc,II}} = \min \left[ f_{\text{esc},10} \left( \frac{M_h}{10^{10} M_\odot} \right)^{\alpha_{\text{esc}}}, 1 \right], \quad (14)$$

$$f_{\text{esc,III}} = \min \left[ f_{\text{esc},7} \left( \frac{M_h}{10^7 M_\odot} \right)^{\alpha_{\text{esc}}}, 1 \right], \quad (15)$$

here  $f_{\text{esc},10}$  and  $f_{\text{esc},7}$   $\alpha_{\text{esc}}$  are free parameters, and we fix  $\alpha_{\text{esc}} = -0.3$  following Muñoz et al. (2022).  $f_{\text{esc}}$  affects the 21cm signal primarily by regulating reionization, which determines the neutral fraction  $x_{\text{H}}$  in Eq. (1). A higher  $f_{\text{esc}}$  accelerates reionization, thereby suppressing the 21cm signal amplitude.

## 3. Forecast Pipeline

### 3.1. Sky temperature and foreground models

The sky-averaged radio data  $T_{\text{sky}}$  (hereafter referred to as the sky temperature) measured by global 21 cm experiments contain the combined contributions of the cosmic signal  $T_{21}$  and the foreground (FG) temperature  $T_{\text{FG}}$  (Tauscher et al. 2020; Cang et al. 2025),

$$T_{\text{sky}} = T_{21} + T_{\text{FG}}. \quad (16)$$

We model the FG temperature using a log-polynomial model (Murray et al. 2022; Cang et al. 2025),

$$T_{\text{FG}} = \left( \frac{\nu}{75 \text{MHz}} \right)^{-\beta} \sum_{i=0}^{N_{\text{FG}}-1} p_i \left[ \ln \left( \frac{\nu}{75 \text{MHz}} \right) \right]^i, \quad (17)$$

where the frequency  $\nu$  is related to redshift by  $z = 1.42 \text{GHz}/\nu - 1$ .  $\beta$  is the spectrum power index which we fix to 2.53 (Jester & Falcke 2009).  $N_{\text{FG}}$  is the number of FG terms, we adopt a five-term FG model and thus set  $N_{\text{FG}} = 5$ .  $p_i$  are fitting coefficients which we will vary in our forecast.

### 3.2. Mock data and choice of fiducials

As with Eq. (16), our mock data can be expressed as the sum of fiducial cosmic 21cm signal  $T_{21,\text{data}}$  and FG temperature  $T_{\text{FG},\text{data}}$ ,

$$T_{\text{sky,data}} = T_{21,\text{data}} + T_{\text{FG,data}}, \quad (18)$$

We compute  $T_{21,\text{data}}$  by setting  $\sigma_0 = 0$  and adopting the fiducial astrophysical parameters from the EOS (Evolution of 21-cm Structure) simulation (Muñoz et al. 2022), which have been shown to be consistent with observations of galaxy UV luminosity functions (UVLFs) and the reionization history. Following Jester & Falcke (2009); Zhao et al. (2025), we produce our mock FG by,

$$T_{\text{FG,data}} = 1697.81 \left( \frac{\nu}{75 \text{MHz}} \right)^{-2.53} \text{K} \quad (19)$$

which corresponds to  $p_0 = 1697.81 \text{K}$  and  $p_i = 0$  ( $i > 0$ ) in Eq. (17).

### 3.3. Specifications of Hongmeng experiment

The Hongmeng mission will be conducted by a ten-satellite array operating in lunar orbit (Chen et al. 2019; Shi et al. 2022; Chen et al. 2023). One of the major goals of Hongmeng is to measure global 21cm spectrum across 30-120 MHz frequencies, this corresponds to a redshift window of  $z \in [10.8, 46.3]$  which we adopt throughout our subsequent data analysis. This task will be undertaken by one of the ten satellites, whereas the rest of the satellites focus on mapping the sky below 30 MHz, collecting data, and communication with Earth.

Following Shi et al. (2022), we model the experimental noise  $\sigma_n$  for Hongmeng by,

$$\sigma_n = \frac{T_{\text{sky,data}} + T_{\text{rcv}}}{\sqrt{\Delta\nu f_{\text{eff}} T_{\text{obs}}}} \quad (20)$$

here  $\Delta\nu = 0.4 \text{MHz}$  is the channel bandwidth.  $T_{\text{obs}}$  is the observation time, and we introduced an observation efficiency parameter  $f_{\text{eff}}$  which is determined by observational strategy. One of the main advantages of conducting 21cm experiments on the lunar orbit is that Earth can be used as a shield against RFI contamination, here we adopt a conservative observational strategy in which the measurement of 21cm signal is only conducted when both the Earth and the Sun are shielded by the Moon, this gives an observation efficiency of  $f_{\text{eff}} = 0.1$  (Shi et al. 2022). The full Hongmeng mission will last for 5 years, and in our analysis we will consider different observation time scales to showcase the expected scientific outputs at different mission stages.

Finally in Eq. (20)  $T_{\text{rcv}}$  is the receiver noise. For Hongmeng instruments, it is given by (Shi et al. 2022),

$$T_{\text{rcv}} = 200 \text{K} \times \left[ 16.809 \exp \left( -\frac{((\nu/75 \text{MHz}) - 0.4)^{1.277}}{0.0808} \right) + 1.034 \right]. \quad (21)$$

### 3.4. Fisher analysis

We use a Gaussian likelihood  $\mathcal{L}$  to model the data distribution for Hongmeng experiment,

$$\ln \mathcal{L} = -\frac{1}{2} \sum \left[ \frac{(T_{\text{sky,data}} - T_{\text{sky,model}})^2}{\sigma_n^2} + 2 \ln \sigma_n \right] + \text{const}, \quad (22)$$

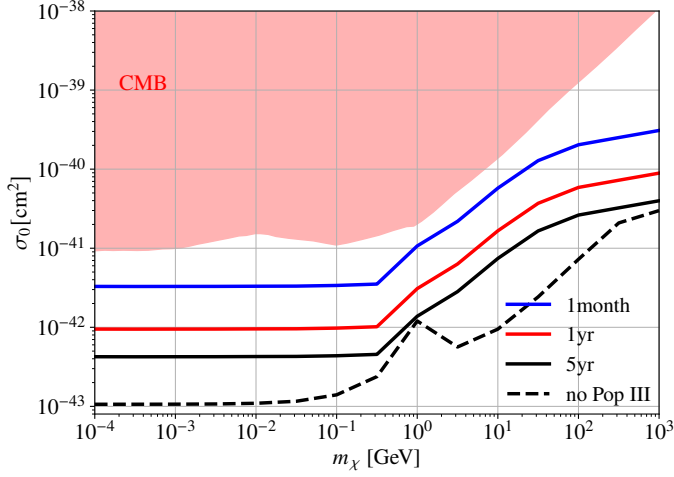


**Fig. 1.** 95% C.I. upper limits on DM-baryon scattering cross-section  $\sigma_0$ . The blue and red solid lines assume observation times of one month and one year respectively, the black solid line shows the results for full mission which lasts for five years. The black dashed line shows expected five-year limits varying only the parameters for Pop II galaxies. Current exclusion bound from CMB (Nguyen et al. 2021) is shown with red shaded regions.

where the summation is over all frequency bands covered by Hongmeng,  $T_{\text{sky,data}}$  is the mock data for the measured sky temperature (see Sect. 3.2),  $T_{\text{sky,model}}$  is the sky temperature computed for different 21cm and FG model parameters. We use the Fisher formalism to estimate the expected uncertainties on SDM cross-section  $\sigma_0$ . Specifically our Fisher matrix  $\mathcal{F}$  can be written as,

$$\mathcal{F}_{ij} = \sum_{\nu} \frac{1}{\sigma_n^2} \frac{\partial T_{\text{sky}}}{\partial \theta_i} \frac{\partial T_{\text{sky}}}{\partial \theta_j} \quad (23)$$

where  $\theta_i$  denotes model parameters. The prospective 68% confidence interval (C.I.)  $\sigma_i$  of parameter  $\theta_i$  can be derived from the Fisher matrix by  $\sigma_i = \sqrt{(\mathcal{F}^{-1})_{ii}}$ .

In total, we vary the following 21cm and FG parameters,

$$\{f_{\star,10}, \alpha_{\star,\text{II}}, f_{\star,7}, \alpha_{\star,\text{III}}, \mathcal{L}_{\text{X,II}}, \mathcal{L}_{\text{X,III}}, f_{\text{esc},10}, f_{\text{esc},7}, \sigma_0, p_{\text{FG},0-4}\} \quad (24)$$

The first four affects the star formation rate. The fifth and sixth determines the overall strength of X-ray radiation, and the seventh and eighth affect the escape fraction of the ionizing photons. The dark matter *physical* parameter is the ninth ( $\sigma_0$ ) and the rest five parameters are the foreground parameters. For convenience, we summarize all these parameters and their fiducial values in Table 1. All our simulations use the same random seed and are run in a box of volume  $200 \text{ cMpc}^3$  with a resolution of  $50^3$ . Apart from the astrophysical and SDM parameters listed above, all other parameters are fixed to their default values in 21cmFirstCLASS.

## 4. Results

We repeat our Fisher forecast over a range of SDM masses to determine the corresponding constraints on  $\sigma_0$ . Fig. 1 shows our forecasted 95% C.I. constraints on  $\sigma_0$ . The blue and red solid curves assume observation time of one month and one year, respectively, whereas the black solid line shows the result assuming the full mission duration of five years. It can be seen that

after the full mission, Hongmeng can tighten the SDM limits by a factor of 21 compared to the current leading CMB constraints (Nguyen et al. 2021), reaching  $\sigma_0 \lesssim 4.3 \times 10^{-43} \text{ cm}^2$  for  $0.1 \text{ MeV} \lesssim m_\chi \lesssim 0.3 \text{ GeV}$ . With a more modest observation time of one year, these limits relax by about a factor of 2.2, yet remain roughly an order of magnitude tighter than the CMB bounds. Even with an observation time of only one month, Hongmeng can already achieve a factor of three improvement over the current CMB limits.

As pointed out in Muñoz et al. (2015), at low SDM masses ( $m_\chi \lesssim 1 \text{ GeV}$ ), the SDM contribution to IGM temperature evolution equation, i.e., Eq. (5), is dominated by near mass-independent cooling, thus our  $\sigma_0$  constraints are flat below  $0.3 \text{ GeV}$ . In the opposite regime ( $m_\chi \gtrsim 1 \text{ GeV}$ ), the second term of Eq. (5) dominate and SDM turns to heat the IGM at a rate which roughly scales as  $dT_k/dt \propto \sigma_0/m_\chi$ , therefore above  $0.3 \text{ GeV}$  our constraints scales roughly as  $\sigma \propto m_\chi$ .

Fig. 2 shows the forecasted constraints on the astrophysical parameters, the foreground parameters, and  $\sigma_0$  for the full Hongmeng mission assuming  $m_\chi = 0.1 \text{ MeV}$ . Apart from  $\sigma_0$  which assumes unit  $10^{-42} \text{ cm}^2$ , in both figures all parameters assume the units and parameterization (linear or  $\log_{10}$ ) listed in Table 1. Accumulation of ionizing UV radiation only causes noticeable impacts on  $x_{\text{H}}$  and consequently on 21cm signal during the epoch of reionization (EoR), which begins around  $z \approx 10$  in our fiducial settings. Such redshifts are not well probed by Hongmeng which targets  $11 \leq z \leq 46$ , therefore one sees from the green contours in Fig. 2 that constraints on  $f_{\text{esc},10}$  and  $f_{\text{esc},7}$  are much weaker compared to that for SFR and X-ray parameters.

Formation of the first generation of galaxies, i.e., Pop III, occurs much earlier than Pop II. Therefore, Pop III galaxies begin affecting the 21cm signal and  $T_{\text{sky}}$  at much higher redshifts, and their influence spans a wider redshift and frequency range probed by Hongmeng. Consequently, Fig. 2 shows that the prospective constraints on Pop III parameters are significantly tighter than those for Pop II. Furthermore, the epoch during which SDM affects the 21cm signal overlaps more substantially with Pop III than with Pop II, leading to a tighter correlation between SDM and Pop III parameters.

To showcase the impact of this tighter correlation between Pop III and SDM, in the black dashed line in Fig. 1 we show the expected full-mission  $\sigma_0$  constraints when Pop III parameters are fixed to their fiducial values, and we find that this gives a tighter (by a factor of 5) and yet potentially less robust constraints. Fig. 2 also shows that without jointly varying Pop III parameters, constraints on Pop II parameters are tightened significantly.

As we briefly discussed in Sect. 2.1, SDM can either cool or heat SDM. We explore this issue further in Fig. 3, in which we show distribution of  $\chi^2 \equiv (T_{\text{sky,data}} - T_{\text{sky,model}})^2 / \sigma_n^2$  over different  $\sigma_0$  and  $m_\chi$  values while keeping the rest of the parameters fixed to their fiducial values. The vertical and horizontal hatches indicate regions where SDM consistently cools and heats the IGM, respectively, within  $11 \leq z \leq 46$ . It can be seen that as mentioned in Muñoz et al. (2015), at  $m_\chi < 10 \text{ MeV}$  SDM consistently leads to extra cooling irrespective to  $\sigma_0$ , and at higher masses SDM starts to heat IGM in some redshifts. Around  $1 \text{ GeV}$ , SDM transitions to consistently heat IGM for  $\sigma_0 \lesssim 10^{-42} \text{ cm}^2$ . Around the mass scale where SDM transitions from cooling to heating, its impact on the 21cm signal is minimized, weakening the  $\sigma_0$  constraints relative to neighboring masses. This produces the bump in the black solid curve at  $1 \text{ GeV}$  in Fig. 1.

The transition of SDM from cooling to heating is dependent not only on SDM mass but also scattering cross-section  $\sigma_0$ . It can be seen from Fig. 3 that, for fixed  $m_\chi$  our  $\chi^2$  shows non-

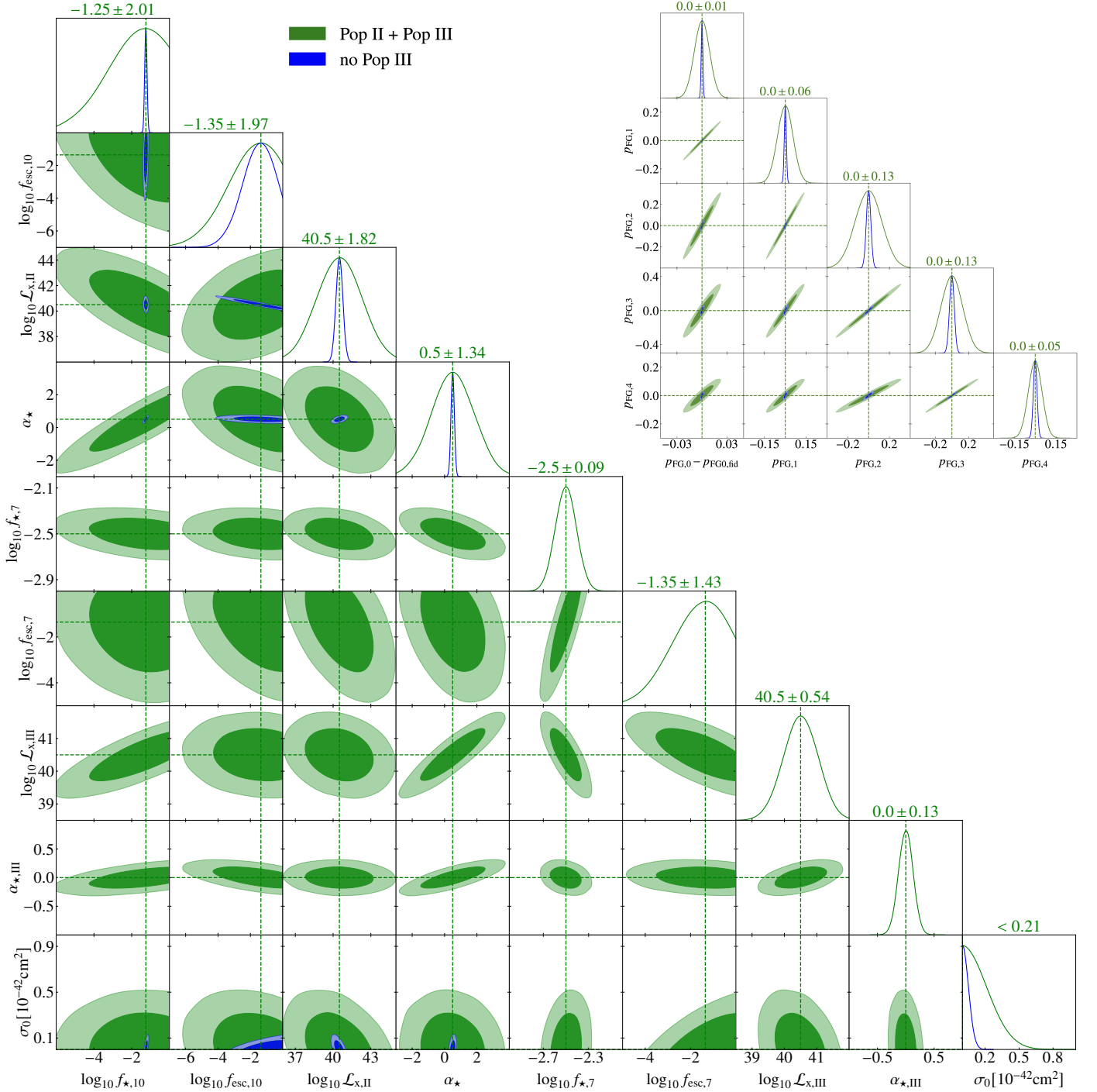


**Fig. 2.** Prospective constraints on astrophysical parameters, FG parameters, and  $\sigma_0$ . We assumed five year observation time and  $m_\chi$  is fixed to 0.1 MeV. The dark and light shaded regions indicate 68% and 95% confidence intervals, respectively. The green contours shows the case in which we jointly vary both Pop II and Pop III parameters (Pop II + Pop III), whereas in blue contours we fixed Pop III parameters ( $f_{\star,7}$ ,  $f_{\text{esc},7}$ ,  $\mathcal{L}_{x,\text{III}}$  and  $\alpha_{\star,\text{III}}$ ) to their fiducial values. Note that constraints on Pop II, FG and  $\sigma_0$  are all significantly tightened when ignoring Pop III parameters. The green dashed line shows the input fiducial values for each parameter, the titles show the 68% limits from the Pop II + Pop III joint analysis. In the upper right panels in which we show constraints for FG parameters,  $p_{\text{FG},0,\text{fid}} = 1697.81\text{K}$  is the fiducial values for  $p_{\text{FG},0}$ .

monotonic behavior when varying  $\sigma_0$ , i.e., around the cross-section where SDM transitions between cooling and heating, the effects of SDM on 21cm is minimized and a local  $\chi^2$  minimum can appear. The likelihood can thus have complex non-Gaussian behavior and become multi-modal. We showcased this effect for fixed astrophysical and FG parameters, however from Eq. (5) one can see that the relative weight between heating and cooling terms depends also on IGM temperature  $T_k$  which is also dependent on

background astrophysics, therefore the presence and location of this local  $\chi^2$  minimum might also be dependent on astrophysical parameters as well.

This multi-modality can potentially have hazardous implications for inference analysis of real 21cm data. Even for the case in which the true value of  $\sigma_0$  is located at 0, one can potentially get biased inference result depending on the sampling strategy, complexity of background astrophysical and FG parameters. For

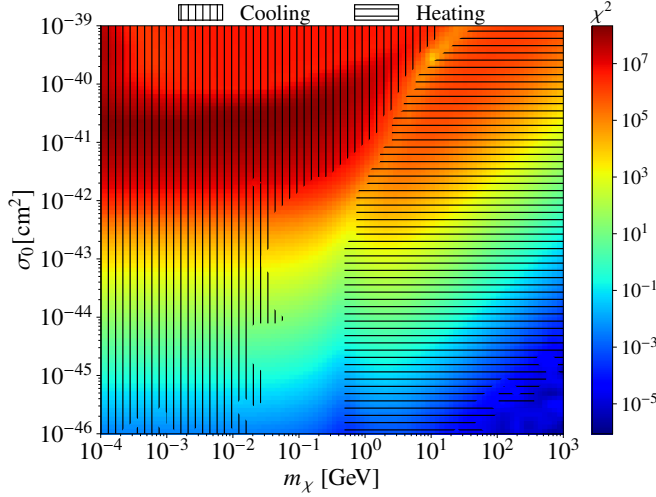


**Fig. 3.** Effects of SDM parameters on IGM temperature and on our likelihood. Color coding represents the value of  $\chi^2 \equiv (T_{\text{sky,data}} - T_{\text{sky,model}})^2 / \sigma_n^2$ . Vertical and horizontal hatches identify regions where SDM consistently cool or heat IGM during  $11 \lesssim z \lesssim 46$ .

example, if one samples  $\sigma_0$  in log space, these local likelihood peaks may be under-weighted and effectively disregarded if their widths are sufficiently narrow in log space. In contrast, sampling  $\sigma_0$  in linear space can make the same local peak appear much broader, and when one include additional parameters for astrophysical background and FG, its height can become indistinguishable compared to that of the true peak. This can over-weight the local maximum and potentially lead to a false SDM detection.

While the Fisher formalism used in this work is fast and enables exploration of a large set of astrophysical parameters, it cannot capture likelihood multi-modalities. Methods such as nested sampling or Markov chain Monte Carlo (MCMC) can resolve these features and yield more reliable parameter constraints. However, they are computationally prohibitive for the large set of astrophysical parameters considered here, so we leave a full analysis to future work.

## 5. Discussions

This paper explores the potential of the Hongmeng 21cm experiment in probing SDM - baryon interactions. We jointly model the contributions to observed sky temperature from SDM, astrophysical background, and foreground. Hongmeng is designed to operate on lunar orbit which allows it to use the Moon to shield Earth RFI contaminations, and we show that even with a very conservative observation strategy in which the experiment operate when both the Earth and Sun are shielded by the Moon, Hongmeng can tighten current leading SDM limits from CMB by a factor of three after just one month of observation. After the five-year full mission, Hongmeng can tighten CMB limits by a factor of 21, reaching  $\sigma_0 \lesssim 4 \times 10^{-43} \text{ cm}^2$  for SDM masses below 0.1 GeV.

In addition to the conventional pop II galaxies, in our astrophysical background we also accounted for the first generation pop III galaxies which might be present at the high redshifts targeted by Hongmeng. We jointly model the star formation, X-ray and UV radiation fields of both galaxy populations to derive robust SDM constraints, and we found that ignoring pop III galaxies

can give much tighter (by about a factor of 5) and yet less robust SDM constraints.

Depending on SDM properties and IGM thermal states, SDM can either cool or heat IGM, as seen in Fig. 3. This leaves a caveat that a scan across these regimes can lead to non-Gaussian behavior in likelihood which is not fully captured by a Fisher analysis. Complicated likelihood behavior can result in multi-modality which potentially results in false detection in inference analysis of real 21cm data, which we postpone to future studies.

## Data Availability

Data used in this work are available upon request to the corresponding author.

*Acknowledgements.* The authors thank Xuelei Chen, Jordan Flitter and Yuewei Wen for helpful discussions. J.C. is thankful to NAOC for hospitality during his visit that initiated this study. Y.G. is partially supported by NSFC under grant no. 12275278. Y.-Z. Ma acknowledges the support from South Africa's National Research Foundation under Grants No. 150580, No. CHN22111069370, No. ERC250324306141.

## References

- Abdurashidova, Z. et al. 2022, *Astrophys. J.*, 924, 51
- Aghanim, N. et al. 2020, *Astron. Astrophys.*, 641, A6, [Erratum: *Astron. Astrophys.* 652, C4 (2021)]
- Barkana, R. 2018, *Nature*, 555, 71
- Barkana, R., Outmezguine, N. J., Redigolo, D., & Volansky, T. 2018, *Phys. Rev. D*, 98, 103005
- Berlin, A., Hooper, D., Krnjaic, G., & McDermott, S. D. 2018, *Phys. Rev. Lett.*, 121, 011102
- Bevins, H. T. J., Fialkov, A., de Lera Acedo, E., et al. 2022, *Nature Astron.*, 6, 1473
- Blas, D., Lesgourgues, J., & Tram, T. 2011, *JCAP*, 07, 034
- Boddy, K. K. & Gluscevic, V. 2018, *Phys. Rev. D*, 98, 083510
- Boddy, K. K., Gluscevic, V., Poulin, V., et al. 2018, *Phys. Rev. D*, 98, 123506
- Boddy, K. K., Krnjaic, G., & Moltner, S. 2022, *Phys. Rev. D*, 106, 043510
- Bowman, J. D., Rogers, A. E. E., Monsalve, R. A., Mozdzen, T. J., & Mahesh, N. 2018, *Nature*, 555, 67
- Burns, J., Hallinan, G., Chang, T.-C., et al. 2021, *arXiv e-prints*, arXiv:2103.08623
- Burns, J. et al. 2021 [arXiv:2103.08623]
- Burns, J. O. et al. 2017, *Astrophys. J.*, 844, 33
- Cang, J., Mesinger, A., Murray, S. G., et al. 2025, *Astron. Astrophys.*, 698, A152
- Chen, X., Yan, J., Deng, L., et al. 2020, *Phil. Trans. Roy. Soc. Lond. A*, 379, 20190566
- Chen, X., Yan, J., Xu, Y., et al. 2023, *Chinese Journal of Space Science*, 43, 43
- Chen, X. et al. 2019, in *ISSI-BJ Forum: Discover the Sky by Longest Wavelength with Small Satellite Constellation*
- Das, A., Mesinger, A., Pallottini, A., Ferrara, A., & Wise, J. H. 2017, *Mon. Not. Roy. Astron. Soc.*, 469, 1166
- Driskell, T., Nadler, E. O., Mirocha, J., et al. 2022, *Phys. Rev. D*, 106, 103525
- Dvorkin, C., Blum, K., & Kamionkowski, M. 2014, *Phys. Rev. D*, 89, 023519
- Ewall-Wice, A., Chang, T. C., Lazio, J., et al. 2018, *Astrophys. J.*, 868, 63
- Ewall-Wice, A., Chang, T.-C., & Lazio, T. J. W. 2020, *Mon. Not. Astron. Soc.*, 492, 6086
- Falkowski, A. & Petraki, K. 2018 [arXiv:1803.10096]
- Feng, C. & Holder, G. 2018, *Astrophys. J. Lett.*, 858, L17
- Fialkov, A. & Barkana, R. 2019, *Mon. Not. Roy. Astron. Soc.*, 486, 1763
- Fialkov, A., Barkana, R., & Cohen, A. 2018, *Phys. Rev. Lett.*, 121, 011101
- Flitter, J. & Kovetz, E. D. 2024, *Phys. Rev. D*, 109, 043512
- Fragos, T., Lehmer, B. D., Naoz, S., Zezas, A., & Basu-Zych, A. R. 2013a, *Astrophys. J. Lett.*, 776, L31
- Fragos, T. et al. 2013b, *Astrophys. J.*, 764, 41
- Furlanetto, S. & Briggs, F. 2004, *New Astron. Rev.*, 48, 1039
- Furlanetto, S., Oh, S. P., & Briggs, F. 2006, *Phys. Rept.*, 433, 181
- Gessey-Jones, T., Fialkov, A., Acedo, E. d. L., Handley, W. J., & Barkana, R. 2023, *Mon. Not. Roy. Astron. Soc.*, 526, 4262
- Gluscevic, V. & Boddy, K. K. 2018, *Phys. Rev. Lett.*, 121, 081301
- Greenhill, L. J. & Bernardi, G. 2012, *arXiv e-prints*, arXiv:1201.1700
- He, A., Ivanov, M. M., An, R., & Gluscevic, V. 2023, *Astrophys. J. Lett.*, 954, L8
- Hibbard, J. J., Rapetti, D., Burns, J. O., Mahesh, N., & Bassett, N. 2023, *Astrophys. J.*, 959, 103

- Hill, J. C. & Baxter, E. J. 2018, JCAP, 08, 037
- Hills, R., Kulkarni, G., Meerburg, P. D., & Puchwein, E. 2018, Nature, 564, E32
- Hirata, C. M. 2006, Mon. Not. Roy. Astron. Soc., 367, 259
- Jester, S. & Falcke, H. 2009, New Astron. Rev., 53, 1
- Karwal, T. & Kamionkowski, M. 2016, Phys. Rev. D, 94, 103523
- Kovetz, E. D., Poulin, V., Gluscevic, V., et al. 2018, Phys. Rev. D, 98, 103529
- Lin, Y. & Gao, Y. 2026, Chin. Phys. C, 50, 015104
- Liu, H. & Slatyer, T. R. 2018, Phys. Rev. D, 98, 023501
- McDermott, S. D., Yu, H.-B., & Zurek, K. M. 2011, Phys. Rev. D, 83, 063509
- Mellema, G. et al. 2013, Exper. Astron., 36, 235
- Mesinger, A., Furlanetto, S., & Cen, R. 2011, Mon. Not. Roy. Astron. Soc., 411, 955
- Mirocha, J. & Furlanetto, S. R. 2019, Mon. Not. Roy. Astron. Soc., 483, 1980
- Muñoz, J. B., Dvorkin, C., & Loeb, A. 2018, Phys. Rev. Lett., 121, 121301
- Muñoz, J. B., Kovetz, E. D., & Ali-Haïmoud, Y. 2015, Phys. Rev. D, 92, 083528
- Muñoz, J. B. & Loeb, A. 2018, Nature, 557, 684
- Muñoz, J. B., Qin, Y., Mesinger, A., et al. 2022, Mon. Not. Roy. Astron. Soc., 511, 3657
- Murray, S. G., Bowman, J. D., Sims, P. H., et al. 2022, Mon. Not. Roy. Astron. Soc., 517, 2264
- Murray, S. G., Greig, B., Mesinger, A., et al. 2020, J. Open Source Softw., 5, 2582
- Nelander, A., Cain, C., DSilva, J. C. J., et al. 2025 [arXiv:2507.21230]
- Nguyen, D. V., Sarnaik, D., Boddy, K. K., Nadler, E. O., & Gluscevic, V. 2021, Phys. Rev. D, 104, 103521
- Park, J., Mesinger, A., Greig, B., & Gillet, N. 2019, Mon. Not. Roy. Astron. Soc., 484, 933
- Pritchard, J. R. & Loeb, A. 2012, Rept. Prog. Phys., 75, 086901
- Qin, Y., Mesinger, A., Park, J., Greig, B., & Muñoz, J. B. 2020, Mon. Not. Roy. Astron. Soc., 495, 123
- Rahimieh, A., Parashari, P., & Gluscevic, V. 2025, Mon. Not. Roy. Astron. Soc., 542, 1605
- Reis, I., Fialkov, A., & Barkana, R. 2020, Mon. Not. Roy. Astron. Soc., 499, 5993
- Riess, A. G. et al. 2018, Astrophys. J., 855, 136
- Shen, E., Anstey, D., de Lera Acedo, E., Fialkov, A., & Handley, W. 2021, Mon. Not. Roy. Astron. Soc., 503, 344
- Shi, Y., Deng, F., Xu, Y., et al. 2022, Astrophys. J., 929, 32
- Short, K., Bernal, J. L., Boddy, K. K., Gluscevic, V., & Verde, L. 2022 [arXiv:2203.16524]
- Sims, P. H. & Pober, J. C. 2020, Mon. Not. Roy. Astron. Soc., 492, 22
- Singh, S., Nambissan T., J., Subrahmanyam, R., et al. 2022, Nature Astron., 6, 607
- Sitwell, M., Mesinger, A., Ma, Y.-Z., & Sigurdson, K. 2014, MNRAS, 438, 2664
- Slatyer, T. R. & Wu, C.-L. 2018, Phys. Rev. D, 98, 023013
- Tauscher, K., Rapetti, D., & Burns, J. O. 2018, JCAP, 12, 015
- Tauscher, K., Rapetti, D., & Burns, J. O. 2020, Astrophys. J., 897, 132
- van Haarlem, M. P. et al. 2013, Astron. Astrophys., 556, A2
- Vedantham, H. K., Koopmans, L. V. E., de Bruyn, A. G., et al. 2014, Mon. Not. Roy. Astron. Soc., 437, 1056
- Xu, W. L., Dvorkin, C., & Chael, A. 2018, Phys. Rev. D, 97, 103530
- Zhao, M.-L., Wang, S., & Zhang, X. 2025, JCAP, 07, 039